One Earth

Article

Impacts of climate change on methylmercury formation and bioaccumulation in the 21st century ocean

Graphical Abstract

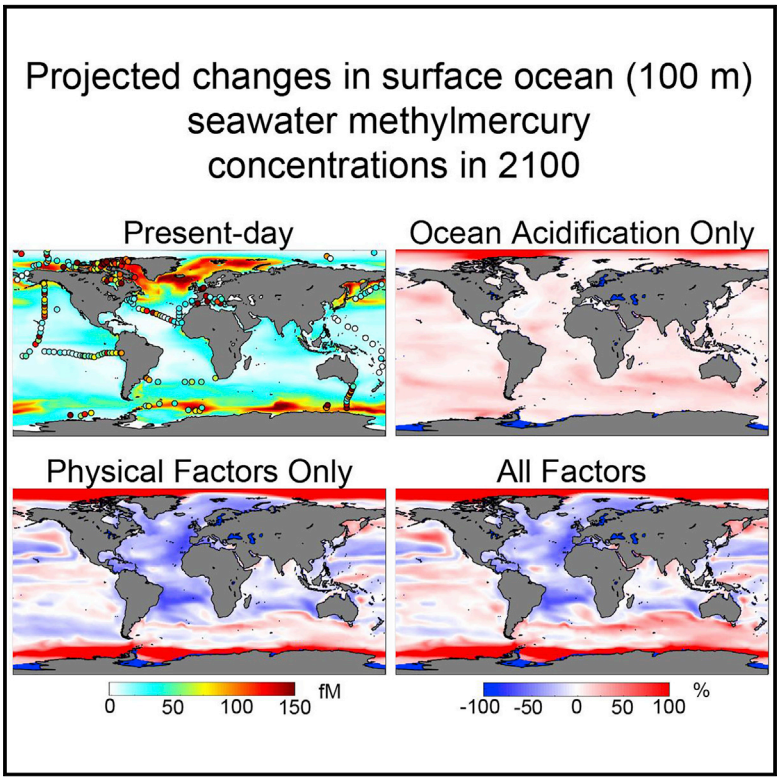

Highlights

- Seawater MeHg may increase in the polar oceans and decrease in the North Atlantic in 2100
- Plankton MeHg may increase at high latitudes and decrease at mid to low latitudes
- Ocean acidification leads to different spatial patterns compared with physical factors

Authors

Yanxu Zhang, Stephanie Dutkiewicz, Elsie M. Sunderland

Correspondence

zhangyx@nju.edu.cn

In Brief

This study projects the influence of climate-induced changes in ocean biogeochemistry on the formation and trophic transfer of neurotoxic methylmercury in 2100. We conclude that large regional variabilities are associated with these changes, and the changes caused by ocean acidification and physical factors have distinct spatial patterns. These effects will affect future trajectories of biological methylmercury concentrations and warrant consideration when measuring temporal trajectories of Hg concentrations in seawater and biota.

Zhang et al., 2021, One Earth *4*, 279–288
February 19, 2021
https://doi.org/10.1016/j.oneear.2021.01.005

CellPress

One Earth

Gold Standard for the Global Goals | 3 tons of CO_2 offset

CellPress

Article

Impacts of climate change on methylmercury formation and bioaccumulation in the 21st century ocean

Yanxu Zhang,[1,5,*] Stephanie Dutkiewicz,[2] and Elsie M. Sunderland[3,4]

[1]School of Atmospheric Sciences, Nanjing University, Nanjing, Jiangsu 210023, China

[2]Department of Earth, Atmospheric and Planetary Sciences, Massachusetts Institute of Technology, Cambridge, MA 02139, USA

[3]Harvard John A. Paulson School of Engineering & Applied Sciences, Harvard University, Cambridge, MA 02138, USA

[4]Department of Environmental Health, Harvard T. H. Chan School of Public Health, Harvard University, Boston, MA 02214, USA

[5]Lead contact

*Correspondence: zhangyx@nju.edu.cn

https://doi.org/10.1016/j.oneear.2021.01.005

SCIENCE FOR SOCIETY Climate change is altering primary production and plankton biomass in the global ocean, which in turn will influence the formation and bioaccumulation of the neurotoxin methylmercury (MeHg). Here we use a model to project how changes in the ocean impact MeHg. Results show an almost doubling of seawater MeHg in the polar oceans and a decrease in the North Atlantic Ocean due to changes in primary productivity. Phytoplankton MeHg may increase at high latitudes and decrease in the mid- and low-latitude oceans due to the shifts in phytoplankton communities. Ocean acidification might enhance the MeHg uptake by phytoplankton by promoting the growth of a small species that efficiently accumulates MeHg. Simulated changes in zooplankton MeHg differ from phytoplankton due to complex grazing relationships. These effects thus need to be considered when evaluating future trajectories of biological MeHg concentrations, including marine fish and shellfish that are consumed by humans.

SUMMARY

Climate change-driven alterations to marine biogeochemistry will impact the formation and trophic transfer of the bioaccumulative neurotoxin methylmercury (MeHg) in the global ocean. We use a 3D model to examine how MeHg might respond to changes in primary production and plankton community driven by ocean acidification and alterations in physical factors (e.g., ocean temperature, circulation). Productivity changes lead to significant increases in seawater MeHg in the polar oceans and a decrease in the North Atlantic Ocean. Phytoplankton MeHg may increase at high latitudes and decrease in lower latitudes due to shifts in community structure. Ocean acidification might enhance phytoplankton MeHg uptake by promoting the growth of a small species that efficiently accumulate MeHg. Non-linearities in the food web structure lead to differing magnitudes of zooplankton MeHg changes relative to those for phytoplankton. Climate-driven shifts in marine biogeochemistry thus need to be considered when evaluating future trajectories in biological MeHg concentrations.

INTRODUCTION

Mercury (Hg) is a global toxicant of concern. Its organic form, monomethylmercury (CH_3Hg), has been associated with neurocognitive deficits in children and impaired cardiovascular health in adults.[1,2] In most countries, human CH_3Hg exposure occurs predominantly through seafood consumption, and thus cycling of CH_3Hg in the ocean is of great interest.[3,4] CH_3Hg in the ocean is mainly formed *in situ* from atmospherically deposited inorganic Hg.[5,6] CH_3Hg efficiently bioaccumulates in marine food webs with the largest magnification between seawater and plankton.[7,8] The first global treaty aimed at reducing anthropogenic Hg releases (the Minamata Convention) entered into force in 2017 (http://mercuryconvention.org). Evaluating the effectiveness of this treaty requires diagnosing the roles of anthropogenic Hg emissions and climate-driven changes for future CH_3Hg exposures.

Excess radiative forcing associated with climate change is leading to increases in global sea surface temperature and altered ocean circulation, with secondary effects on nutrient

and light availability.[9] Higher atmospheric CO_2 concentrations also lead to elevated carbonic acid and a lowering of seawater pH or ocean acidification (a projected drop of about 0.4 pH units by 2100).[10] These changes are expected to substantially alter spatial patterns in primary productivity, carbon remineralization, and phytoplankton community structure,[10,11] thus indirectly affecting CH_3Hg accumulation in food webs.[12] In particular, ocean acidification is expected to change spatial patterns in plankton community composition.[10]

Understanding the effects of climate change on CH_3Hg formation in the marine environment is limited. Booth and Zeller[13] predicted an increase in seawater total methylmercury [MeHg, the sum of CH_3Hg and $(CH_3)_2Hg$] concentrations in a future climate because they assumed inorganic Hg methylation would be enhanced by warmer ocean temperatures.[14] Many studies have shown MeHg formation in the marine water column is associated with the activity of heterotrophic,[15–18] and the expression of the key Hg methylating genes, *hgcAB*, has been found across all ocean basins.[19,20] It has been widely suggested that climate change will exacerbate MeHg production in the future, as higher temperatures facilitate organic carbon remineralization.[5,12,21]

The effects of climate change on CH_3Hg uptake at the base of marine food webs are similarly uncertain. Jonsson et al.[22] suggested that increases in terrestrial dissolved organic matter (DOM) discharges from rivers may elongate the trophic structure of estuarine food webs, leading to higher CH_3Hg concentrations. However, in open ocean regions, DOM concentrations are much more uniform and will not be subject to the same magnitudes of changes as the shelf and slope.[23] Schartup et al.[8] showed that shifts in phytoplankton community composition due to changing ecosystem productivity alter CH_3Hg uptake at the base of marine food webs. As some ecosystems become less productive, phytoplankton communities favor smaller species with larger cell surface area-to-volume ratios that facilitate nutrient and CH_3Hg uptake.[7,8] Prior work has assumed that uptake rates for CH_3Hg increase in warmer seawater.[13,24,25] However, experimental data collected by Lee and Fisher[7] did not show a significant change in CH_3Hg uptake at higher seawater temperatures for most marine phytoplankton species. Instead, the cell surface area-to-volume ratio appears to be the most important factor driving CH_3Hg uptake by phytoplankton,[8] illustrating the importance of potential shifts in phytoplankton community structure.

Impacts of climate-driven changes on CH_3Hg bioaccumulation are known to propagate to higher trophic-level fish.[26] Prior modeling efforts have assumed a temperature-dependent increase in the grazing flux for herbivorous zooplankton under a warmer climate.[13,25] Alava et al.[25] reported such bioenergetic shifts will result in an approximately 12% increase in CH_3Hg concentrations in zooplankton in 2100 under the RCP 8.5 scenario (a high emission scenario often referred to as "business as usual").[27] However, these studies did not consider regional shifts in phytoplankton community structure in a warmer environment that would affect the grazing flux for herbivorous zooplankton, which depends on the biomass of both phytoplankton and zooplankton.[11] These changes also potentially influence the food web dynamics of CH_3Hg.

Here we examine the effects of future changes in ocean biogeochemistry on CH_3Hg concentration in seawater and its bioaccumulation at the base of the marine food webs. We simulate seawater MeHg concentrations and CH_3Hg uptake by marine food webs using a global 3-dimensional model (MITgcm-Hg).[6] The model is driven by the output (e.g., carbon remineralization, plankton biomass, and grazing fluxes) of an ecosystem model (Darwin) that was used to simulate the ecological response to climate change in a "business as usual" emissions scenario over the 21st century.[10] We perform three simulations: (1) a baseline simulation, in which MITgcm-Hg is driven by the output of the Darwin model for the year 2000; (2) a simulation for the year 2100, in which MITgcm-Hg is driven by the projection of the Darwin model as a consequence of changing ocean temperature, circulation, and sea-ice cover (i.e., physical changes) in 2100. We also explore the effects of changing ocean biogeochemistry on MeHg driven by ocean acidification. We do this by conducting (3) a simulation with both physical changes as in (2) and also with pH changes simulated in the work by Dutkiewicz et al.[10] The difference between simulation 2 and 3 is attributed to ocean acidification and is referred to as "ocean acidification only" results. The impact of other climate-change factors (i.e., difference between 2 and 1) is referred to as "physical factors only" results, and the combined effects of all above-mentioned factors (i.e., difference between 3 and 1) are referred to as "all factors" results. We hold both the anthropogenic and natural emissions of Hg constant for the year 2010, as well as the current day circulation for MITgcm-Hg, to diagnose the sensitivity of the changing ocean biogeochemistry and ecology of the future ocean (see Experimental procedures for details).

RESULTS AND DISCUSSION

Changing MeHg concentrations in seawater

We focus on MeHg concentrations because most observational studies report the sum of CH_3Hg and $(CH_3)_2Hg$ in seawater. Modeled seawater MeHg concentrations for the upper 100 m of the water column (surface ocean) in the year 2000 (52 ± 55 fM) are consistent with available observations (67 ± 73 fM) during 1990–2015 (Figure 1A, data are from Zhang et al.,[6] Bowman et al.,[28] and references therein). The modeled concentrations at peak MeHg level depth in the subsurface ocean (350 ± 310 fM, typically 300–500 m depth) also agree with observations (290 ± 280 fM, Figure 1B). For the year 2100, MITgcm-Hg suggests a 9% increase for the global mean seawater MeHg concentrations in the surface ocean (Figure 1G) and 6% decrease at the peak MeHg depth (Figure 1H) as a result of changing ocean biogeochemistry and ecology due to all factors. However, the directionality and magnitude of the projected changes differ substantially for different ocean regions and driving factors (Figures 1C–1F and Table 1).

First, we discuss the impacts of physical factors. In the surface ocean, the model suggests a decline in seawater MeHg concentrations in 2100 in the North and Tropical Atlantic Ocean (33% and 29%, respectively, Figure 1C). This reflects the reduced supply of nutrients projected by the Darwin model due to enhanced ocean stratification and changes in seawater circulation, which decreases primary production and carbon remineralization associated with Hg methylation.[6] In 2100, increases in stratification and reduced nutrient supply, as projected by the Darwin model, result in a shift in the phytoplankton community structure toward smaller size classes (such changes in community

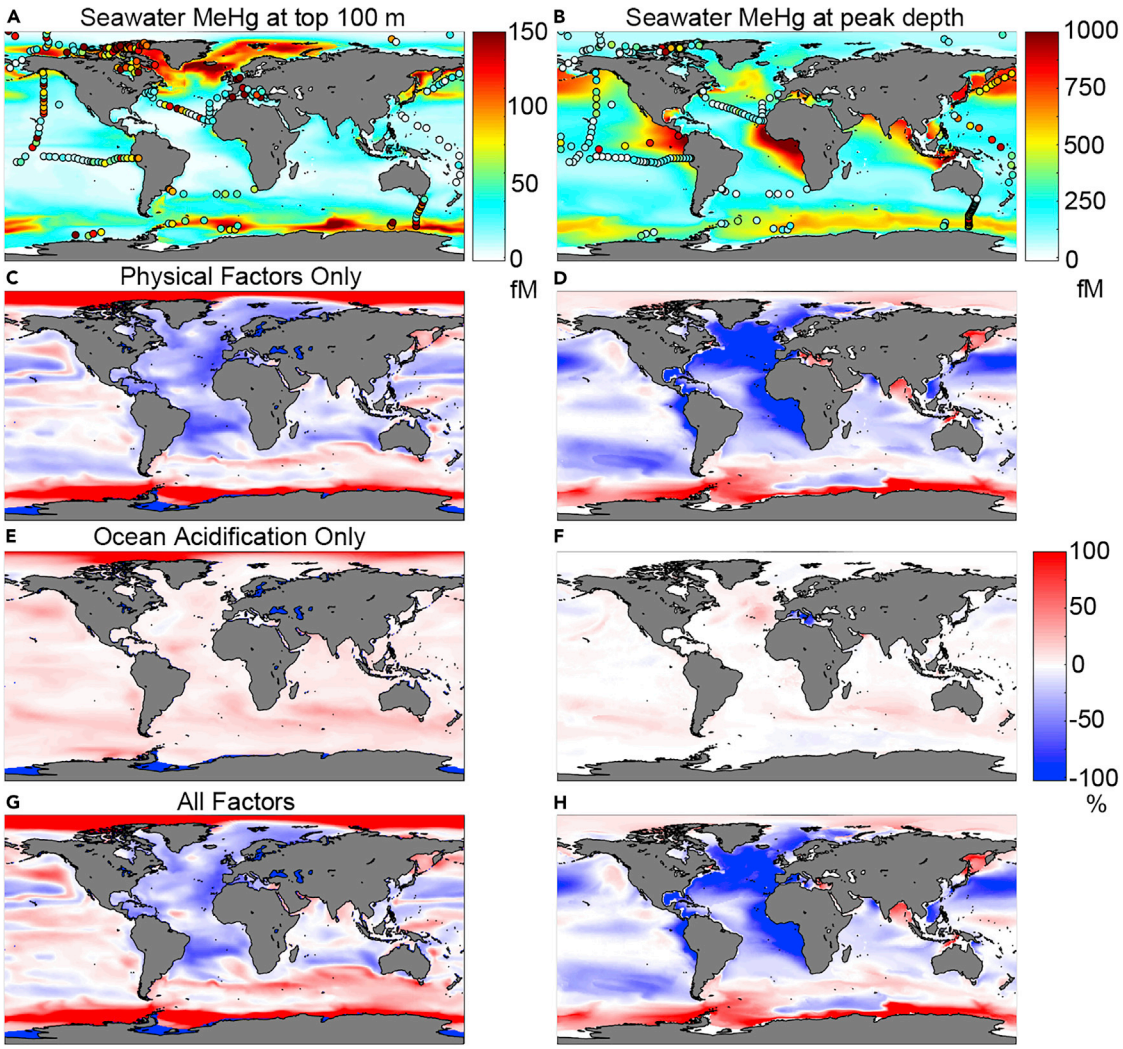

Figure 1. Projected changes in seawater MeHg concentrations in 2100

Modeled seawater MeHg concentrations in the year 2000 ([A] and [B]) and simulated changes in the year 2100 due to shifts in physical factors only ([C] and [D]), ocean acidification only ([E] and [F]), and all factors together ([G] and [H]). Left panels ([A], [C], [E], and [G]) show the top 100 m of seawater, and right panels ([B], [D], [F], and [H]) show concentrations (changes) at the depth of peak seawater MeHg levels. Superimposed circles on (A) and (B) are observations summarized in Zhang et al.[6] and Bowman et al.[28]

structure are typically simulated in climate change marine ecosystem models; e.g., Bopp et al.,[29] Steinacher et al.,[30] Marinov et al.[9]). This diminishes export production at 100 m depth by 20%.[10]

Seawater MeHg concentrations in the surface ocean are projected to increase in both the Arctic (87%, except for the region adjacent to the North Atlantic Ocean) and southern (130%) oceans in the year 2100 due to physical factors (Figure 1C). The Darwin model projects that increasing seawater temperature and altered light environment in the 21st century in the polar regions lead to higher primary productivity and carbon remineralization.[10] The MITgcm-Hg model suggests that this could potentially increase surface ocean MeHg concentrations (Figures 1C and Table 1). Such changes are also likely to be affected by declines in inorganic Hg as the substrate for methylation due to enhanced oceanic evasion in ice-free waters[31–33] and a potential increase in riverine discharge of inorganic Hg and MeHgz from the terrestrial environment due to thawing permafrost.[34–37] However, these changes cannot be quantitatively evaluated as the climate impacts on sea-ice fraction, permafrost dynamics, and riverine Hg discharge are not included in the MITgcm-Hg model.

In contrast to the surface ocean, modeled global mean MeHg concentrations at peak depth are projected to slightly decrease by 6% in 2100 due to physical factors (Figures 1D and S1). However, the modeled changes are spatially heterogeneous with increases or almost no changes over iron-limited regions: e.g., the Southern Ocean (14%) and Tropical Pacific (−4%), as primary production and carbon remineralization over these regions increase as projected by the Darwin model.[10] Declines in subsurface seawater MeHg concentrations are projected for all regions that are limited by dissolved inorganic fixed nitrogen: e.g., North

Table 1. Percentage regional responses to different driving factors in 2100 relative to the present-day conditions

				Plankton[b]					
	Seawater[a]			Phytoplankton		Zooplankton			
Basins	surface	max	diatom	syn	pro	small	large	BCF[f]	ZMF[g]
Arctic	−8[c]	−5	−66	48		169	−36	21	−75
	6[d]	1	45	53		−133	−12	14	−9
	−3[e]	−4	−22	101		35	−48	35	−84
	−33	−30	−61	−29	−40	−39	−77	20	−60
NA	4	2	−13	17	−60	22	−8	7	−12
	−29	−28	−75	−11	−100	−17	−85	28	−72
	−29	−17	−42	−48	−28	−61	−57	29	−25
TA	4	1	−27	27	−72	13	−3	−45	13
	−25	−17	−69	−21	−100	−48	−61	−16	−12
	−1	0	−11	9	−15	−5	−6	−2	0
SA	9	1	−20	54	−85	65	−20	12	−12
	8	1	−30	64	−100	60	−26	11	−12
	−5	−6	−15	−13	−10	−14	−17	17	−6
NP	8	0	−17	29	−90	41	−10	−19	9
	3	−6	−32	16	−100	27	−27	−2	4
	−4	−4	−24	−18	−15	−20	−36	2	−5
TP	5	1	−31	280	−85	15	−18	−54	25
	1	−4	−55	262	−100	−5	−53	−52	21
	−7	−15	−27	−8	5	−14	−32	15	−11
SP	11	4	−23	64	−105	73	−2	−55	39
	4	−11	−50	56	−100	58	−33	−39	28
	1	−3	−7	0	−11	−20	−10	12	−9
Indian	11	2	−28	77	−89	25	−8	−22	−11
	12	−1	−35	77	−100	5	−18	−10	−19
	68	14	61	163	−43		164	−26	23
S	7	0	41	118	−57		−37	12	−41
	75	14	102	281	−100		127	−13	−18
	2	−7	−8	13	−14	−23	−35	7	−26
Global	7	1	−11	64	−86	25	−12	−36	1
	9	−6	−19	77	−100	3	−47	−29	−24

The global ocean is divided into nine basins: Arctic, NA (North Atlantic), TA (Tropical Atlantic), SA (South Atlantic), NP (North Pacific), TP (Tropical Pacific), SP (South Pacific), Indian, and S (Southern) Oceans. Blank values indicate too little biomass to calculate robustly.

[a]For MeHg.

[b]For CH_3Hg.

[c]Changes due to physical factors only.

[d]Changes due to ocean acidification only.

[e]Changes due to all factorsy.

[f]Defined as the ratios of the CH_3Hg concentration in all phytoplankton divided by that in seawater.

[g]Defined as the ratio of the CH_3Hg concentration in herbivorous zooplankton divided by that in phytoplankton.

Atlantic (30%), Tropical Atlantic (17%) (Figure 1D and Table 1). This reflects the modeled reduced remineralization of carbon at the subsurface ocean due to a decline in carbon export,[10] which is used to parameterize microbial activity affecting MeHg formation. The modeled decline in carbon export is driven by less primary production and enhanced efficiency of carbon remineralization at shallower depths due to warmer temperatures (see discussion in Kwon et al.[38]). Although the subsurface maximum MeHg concentrations in the Arctic Ocean are predicted to decrease by 8% in 2100 due to physical factors (Table 1), excluding the part influenced by the North Atlantic Ocean results in an increase of 10%, reflecting the competing effect of projected increased primary production and enhanced carbon remineralization in subsurface waters.

We now consider the effect of ocean acidification. On a global mean basis, the surface seawater MeHg concentrations are simulated to increase by 7% due to ocean acidification only in the year 2100. This reflects modeled higher growth rates of most phytoplankton due to the CO_2 fertilization effect,[39,40] which increases carbon remineralization, bacterial activity, and

modeled MeHg formation. Modeled impacts of ocean acidification on seawater MeHg concentrations are fairly uniform across the global ocean (Figure 1E). The relative increase in MeHg concentrations is close to the mean growth rate increase in phytoplankton growth in response to elevated pCO_2 (partial pressure of CO_2 in seawater, 6%) simulated by the Darwin model.[10]

The modeled impacts of ocean acidification on seawater MeHg concentrations at peak depth are much smaller than physical factors (Figures 1F and S1). Increased pCO_2 was modeled to elevate phytoplankton growth and primary productivity leading to more export production by the Darwin model[10] but only a negligible (1%) increase in concentrations at peak MeHg depth. The modeled impact of ocean biogeochemistry diminishes with depth due to the continuous decrease of remineralization rate for sinking particles,[41] which is associated with Hg methylation (e.g., Sunderland et al.[15]). Moreover, despite large spatial and temporal variability, the average lifetime of MeHg in the surface ocean (top 100 m) and subsurface ocean (100–1000 m depth) is approximately 20 days and 7 years, respectively, compared with 70 years in the deep ocean below 1000-m depth.[6] Longer lifetimes of MeHg in deep waters (>1000-m depth) mean concentrations represent a cumulative function of historical *in situ* production and degradation as well as isopycnal and diapycnal transport over a longer time compared with surface and subsurface waters.[6]

CH_3Hg in phytoplankton

We focus on only CH_3Hg in the marine food web because the potential of $(CH_3)_2Hg$ to bioaccumulate has not been established.[42] The modeled CH_3Hg in phytoplankton generally agrees with available observations at present day (Figures 2 and S2).[6] The global average CH_3Hg reservoirs in phytoplankton in 2100 are projected to increase by 19% as a result of all factors of climate change, with no appreciable change due to physical factors (−0.7%) and larger changes attributable to ocean acidification (20%) (Figure 2). This increase is mainly driven by a projected increase in the biomass of the phytoplankton species, *Synechococcus*, in a lower pH environment (Figures 2G and S4, Dutkiewicz et al.[10]). Experimental studies suggest that the size of phytoplankton cells is the most important factor for the uptake of CH_3Hg from seawater to phytoplankton.[7,43] *Synechococcus* have a small radius and subsequent high surface area-to-volume ratio that enhances CH_3Hg uptake compared to other common marine phytoplankton. Overall, the CH_3Hg in small phytoplankton (*Synechococcus* and *Prochlorococcus*) is projected to increase by 34% in 2100 while the CH_3Hg in large phytoplankton (including diatoms and others) is projected to decrease by 5% due to all factors.

Modeled CH_3Hg reservoirs in different functional groups of phytoplankton have distinct spatial patterns, reflecting the different biogeoprovinces they occupy as projected by the Darwin model (Figure 2 left column). Large spatial variabilities are projected for their responses to ocean acidification and physical factors (Figure 2). Model results suggest declines in phytoplankton CH_3Hg reservoirs in the mid- and low-latitude regions and increases at high latitudes for physical factors (Figure 2, the second column from left, Table 1). For example, the CH_3Hg reservoir in tropical Atlantic and Pacific Oceans are projected to reduce by 28% to 48% and 15% to an increase in 24% for different phytoplankton, respectively (Table 1). This spatial pattern mimics the modeled changes in surface seawater MeHg concentrations in 2100 (Figure 1C). This pattern is also driven by the modeled poleward shifts in the habitats of different functional groups as the ocean warms (Figure S4).[10]

The modeled impact of ocean acidification on CH_3Hg in individual phytoplankton species varies more substantially than physical factors (Figure 2, the third column from left), and dominates the overall pattern for all climate change factors (Figure 2, right column). Ocean acidification is potentially a stronger driver of functional diversity change than physical factors.[10] For larger phytoplankton, ocean acidification amplifies the effects of physical factors because elevated temperature and higher pCO_2 both increase growth in the higher nutrient high latitudes (Figure 2C).[10] Ocean acidification is projected to increase *Synechococcus* biomass nearly everywhere due to enhanced growth rates with elevated pCO_2 compared with other phytoplankton classes, as suggested by the Darwin model. Similar trend is projected for the CH_3Hg reservoir in this phytoplankton (Figure 2G). The model suggests that small phytoplankton (*Prochlorococcus* and *Synechococcus*) dominate the overall uptake of CH_3Hg by phytoplankton in the global oceans due to their large surface area-to-volume ratios. The modeled global increase in CH_3Hg in phytoplankton due to ocean acidification (mean global change of 20%) is mainly driven by the modeled increase in *Synechococcus* biomass (58%) in 2100.

Figure 3 (left column) shows modeled bioconcentration factors (BCF, defined as the ratios of the CH_3Hg concentration in all phytoplankton divided by the concentration in seawater) for 2000 and 2100. The model suggests a strong latitude-dependent pattern for the change of BCF as a result of all factors (Figure 3G). Over low latitudes, the projected increase in *Synechococcus* and decrease in *Prochlorococcus* by the Darwin model overall decrease the average BCF values, as the former is three times larger in size than the latter, which results in a smaller overall surface area-to-volume ratios and less efficient CH_3Hg uptake. For example, the BCF values in Tropical Atlantic and Pacific Oceans are predicted to decrease by 16% and 52%, respectively (Table 1). In the high-latitude oceans, a similar transition is predicted to occur from large eukaryotes to smaller *Synechococcus*, which causes a decrease in BCF values. For instance, the BCF values in the North and South Atlantic Ocean are projected to increase by 28% and 11%, respectively, as a result of all factors.

CH_3Hg in herbivorous zooplankton

Figure 2 (M-T) shows the CH_3Hg distribution in herbivorous zooplankton and their response to climate change. The modeled results at present day are within the range of available observations in the open ocean as summarized by Hammerschmidt et al.[44] and Zhang et al.[6] The modeled global trophic transfer flux for CH_3Hg from phytoplankton to herbivorous zooplankton is 6.2 Mmol/year for the year 2000 (Figure S3). This flux is projected to decrease to 4.7 Mmol/year in 2100 resulting from all factors, while ocean acidification (+0.5 Mmol/year) and physical factors (−2.0 Mmol/year) are operating in opposite directions. The magnitude of changes in CH_3Hg reservoirs in herbivorous zooplankton is similar to that of the trophic transfer flux. Model results suggest a global average decline in CH_3Hg in herbivorous zooplankton attributable to physical factors in 2100 of

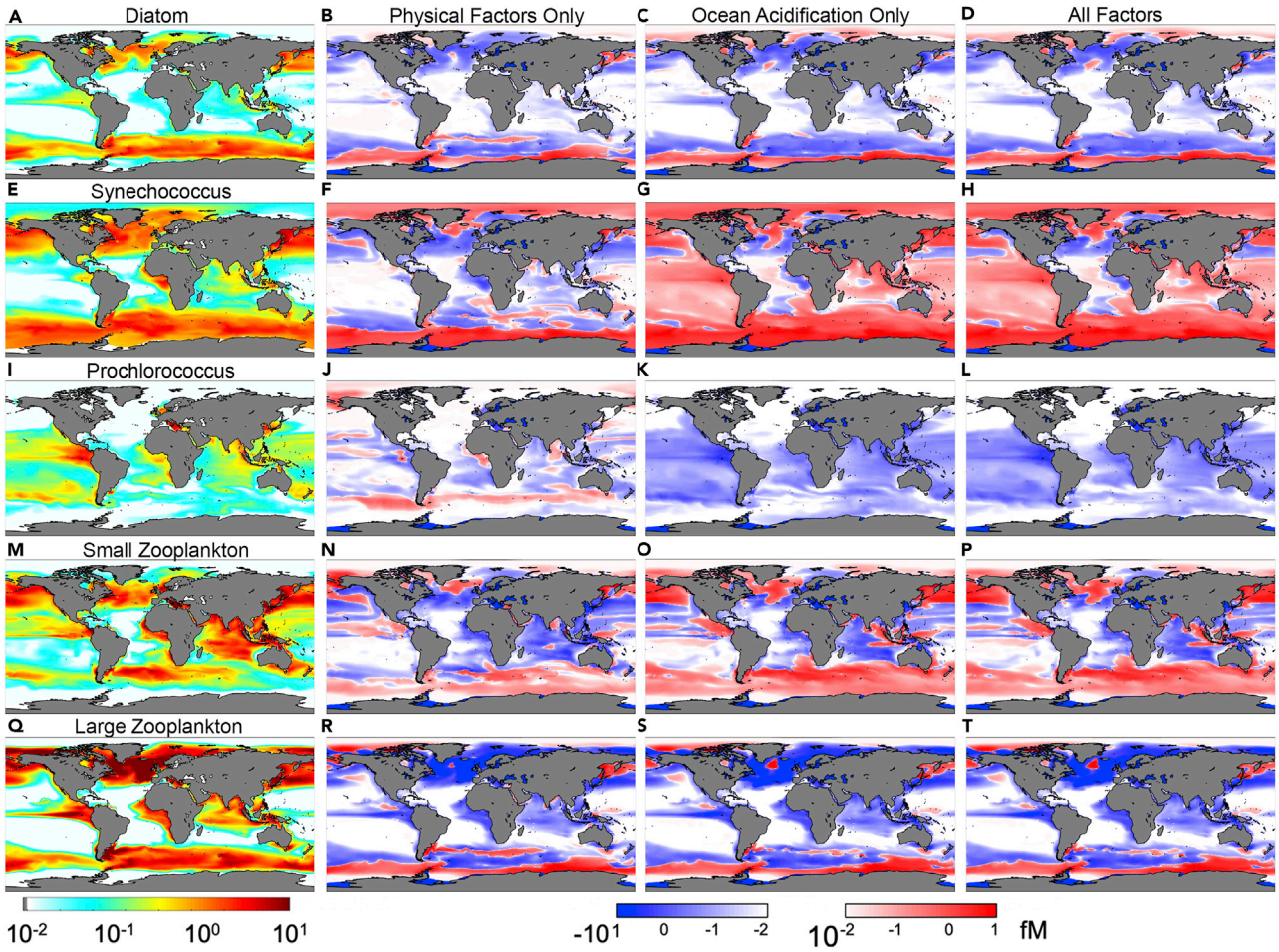

Figure 2. Climate-driven changes in CH_3Hg concentrations in plankton in 2100

Baseline conditions in the year 2000 are shown on the left ([A], [D], [G], [J], and [M]) and compared with changes driven by shifts in physical factors only ([B], [F], [J], [N], and [R]), ocean acidification only ([C], [F], [I], [L], and [O]), and all factors together ([D], [H], [L], [P], and [T]). Results are shown for three functional groups of phytoplankton: Diatoms (diameter = 12 μm; [A]–[C]), *Synechococcus* (*Syn*, 1.8 μm; [D]–[F]), and *Prochlorococcus* (*Pro*, 0.6 μm; [G]–[I]), and small (small zoo., 30 μm; [J]–[L]) and large (large zoo., 100 μm; [M]–[O]) herbivorous zooplankton (results for other phytoplankton are available in Figure S4). Note the log scale of the color bar. Negative changes are indicated by blue and positive changes by red. See also Figure S2.

approximately 30%, and a much smaller increase attributable to ocean acidification of approximately 2%. Again, these link to the opposite signs of primary productivity suggested by the Darwin model for the different altering factors.

The responses of CH_3Hg reservoirs in zooplankton to climate change factors depend on size. Similar to the relative increase in smaller sized phytoplankton projected by the Darwin model, the community structure of herbivorous zooplankton also shifts to the smaller sized category in the future ocean (Figure S4).[10] The CH_3Hg reservoir in small zooplankton is projected to slightly increase by 3%, while to decrease 47% for the large zooplankton due to all factors (Table 1). Spatial changes in CH_3Hg reservoirs for the small and large zooplankton are similar to their biomass, which reflects the availability of their major prey (small zooplankton feed on *Prochlorococcus* and *Synechococcus*; large zooplankton feed on diatoms and other large phytoplankton). Physical factors are modeled to result in an increase in zooplankton in higher latitudes in response to higher phytoplankton concentrations and warmer waters (Figures 2N and 2R). We project a 25% increase for the CH_3Hg reservoir in small zooplankton due to ocean acidification (Figure 2L), which is associated with the projected global increase in *Synechococcus* (Figure 2G).

Forecasted changes in CH_3Hg reservoirs in herbivorous zooplankton in response to all factors (small and large: 3% and −47%, respectively) differ vastly in magnitude from the changes of phytoplankton (34% and −5%, respectively). Similar results are simulated for individual ocean basins (Table 1). This is associated with the nonlinear relationship between zooplankton and phytoplankton biomass. Trophic amplifications have been seen in biomass and production in previous model studies (e.g., Chust et al.[45]). The response of the zooplankton grazing rate to phytoplankton biomass generally follows a Michaelis-Menten type function, and the steepness of this function deviates from one as the phytoplankton biomass are lower or higher than the half-saturation constant.[41,45] This effect is seen here also in the bioaccumulation of Hg. This reinforces the importance of food web dynamics for understanding the impacts of climate change on CH_3Hg bioaccumulation at higher trophic levels.

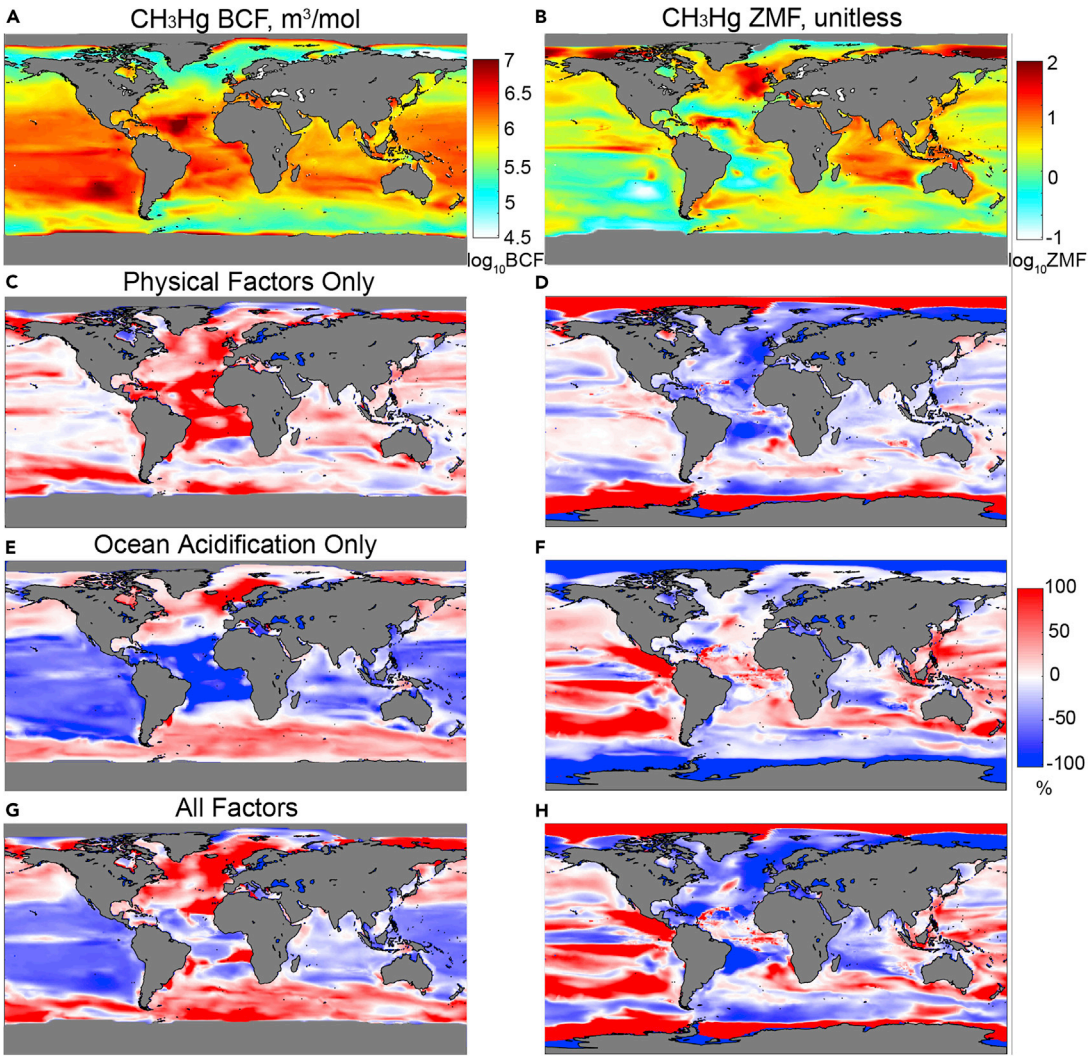

Figure 3. Projected changes in CH_3Hg uptake by phytoplankton and trophic magnification to zooplankton in 2100

Changes in total CH_3Hg uptake by phytoplankton (BCF; [A], [C], [E], and [G]) and trophic magnification to herbivorous zooplankton (ZMF; [B], [D], [F], and [H]) as a result of physical factors only ([C] and [D]), ocean acidification only ([E] and [F]), and all factors together ([G] and [H]), compared with the corresponding values at present day ([A] and [B]).

The modeled global average zooplankton magnification factor (ZMF, defined as the ratio of the CH_3Hg concentration in herbivorous zooplankton divided by that in phytoplankton) in the year 2000 is 4.7 and is forecasted to decrease by 24% in 2100, with ocean acidification (+1%, Figure 3F) and physical factors (−26%, Figure 3D) contributing to the opposite direction. A substantial decrease (32%) in the grazing flux of CH_3Hg resulting from physical factors mainly drives this decline, as discussed above. Although the global average ZMF is predicted to only slightly increase due to ocean acidification (1%, Figure 3F), changes are not uniform globally. The projected shift from *Prochlorococcus* to *Synechococcus* and the increase in small zooplankton results in an increase in the ZMF in the low-latitude ocean regions (e.g., 13% and 25% for Tropical Atlantic and Pacific Ocean, respectively, and 39% for South Pacific Ocean, Table 1). In the high-latitude oceans, the ZMF decreases because of a projected decline in the biomass of eukaryotic phytoplankton and large zooplankton in response to ocean acidification (e.g., 12% in North Atlantic Ocean).

Summary and uncertainty

The results of this study help to diagnose the roles of multiple simultaneously occurring changes in the global oceans. Here we suggest that these changes will affect seawater MeHg concentrations, CH_3Hg uptake, and trophic transfer at the base of marine food webs. These changes are spatially heterogeneous. Our results suggest that the changes in CH_3Hg driven by alterations in physical factors have different patterns than the changes that might occur due to ocean acidification. Our model simulates how future changes in organic carbon export and remineralization will affect shifts in MeHg production rates in the global oceans. These changes reflect spatially variable impacts of increases in primary productivity driven by warming

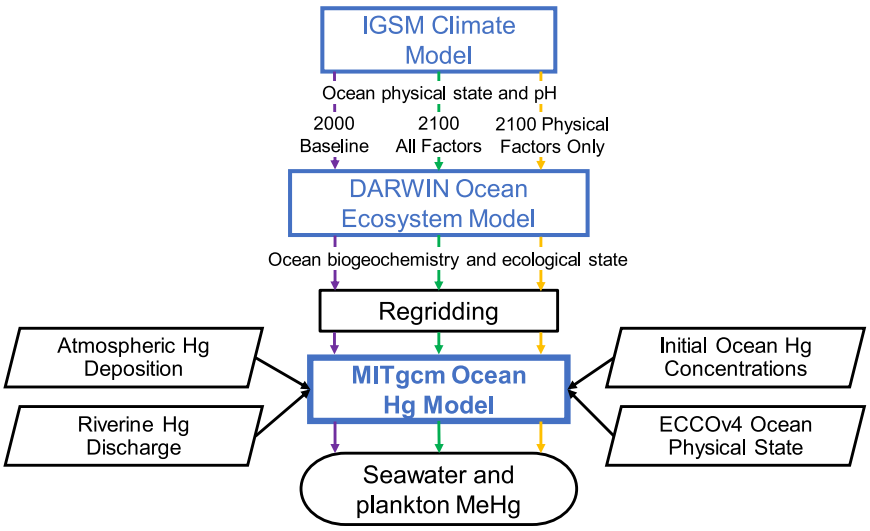

Figure 4. Schematic of the model coupling methodology

The purple, green, and orange arrows are for the present day, all factors, and physical factors only scenarios, respectively.

temperatures and ocean acidification, or decreasing productivity due to increasing ocean stratification and decreased nutrient supply. CH_3Hg reservoirs in the phytoplankton are influenced by phytoplankton community structure. The increase of *Synechococcus* at the expense of larger phytoplankton as a result of ocean acidification is expected to increase CH_3Hg uptake by phytoplankton at the base of the marine food web. Our results suggest that the magnitude of change of CH_3Hg reservoirs in herbivorous zooplankton in the 21st century ocean differ from phytoplankton, reflecting nonlinearity embedded in the food web structure.

Anticipating changes in Hg cycling in the 21st century ocean depends on our understanding of the fundamental processes that drive Hg methylation and food web uptake. The MITgcm-Hg model presented here has been extensively evaluated against observations but contains structural uncertainty due to an incomplete understanding of the processes leading to CH_3Hg formation and bioaccumulation in marine food webs. Nonetheless, it represents a state-of-the-science assessment of multiple interacting processes.[6] Quantitative evaluation of all these parameters is computationally prohibitive, and the overall uncertainty could be represented by the differences between the modeled and observed seawater MeHg concentrations (approximately ±30%). However, some of the model uncertainty can be canceled, as we are analyzing the differences between different simulations. Similarly, there is uncertainty inherent in the ocean biogeochemistry and ecosystem model used to project the 21st century ocean conditions. Model intercomparisons reveal that shifts in primary production in nitrogen-limited regions are robust among models but less consistent in iron-limited regions.[29] Models also agree that the overall fraction of smaller phytoplankton will increase in warming scenarios.[9,30] The response of ocean biogeochemistry and phytoplankton community structure to ocean acidification, on the other hand, is subject to greater uncertainty due to the lack of experimental data on the phytoplankton growth response over the full range of pCO_2 considered and the associated physiological tradeoffs.[10] The results of this study must be understood within this degree of uncertainty of both the projections of the ecosystem change over the 21st century and our ability to include the many components of the Hg cycling.

Predicting the CH_3Hg concentrations in the marine food web has implications for human exposure through seafood consumption. Besides the changes in anthropogenic Hg emissions targeted by the Minamata Convention, our study demonstrates the importance of changing ocean biogeochemistry and ecology in CH_3Hg cycling. Figure 4 shows a flowchart of the models and data used in this study. Overall, this study provides an envelope for shifts in CH_3Hg cycling projected for the 21st century ocean.

EXPERIMENTAL PROCEDURES

Resource availability

Lead contact

Further information and requests for resources and reagents should be directed to and will be fulfilled by the lead contact, Yanxu Zhang (zhangyx@nju.edu.cn).

Materials availability

This study did not generate new unique materials.

Data and code availability

We have included the data and all scripts that replicate the results presented in this study in Mendeley Data: https://doi.org/10.17632/9gr7cd7bhd.1.

Model setup

We use the ocean biogeochemistry and ecosystem results from Dutkiewicz et al.[10] These results were generated by the Darwin marine ecosystem model that is run for 1860 to 2100. The model is based on MITgcm (http://mitgcm.org) and has a resolution of 2 ° × 2.5 ° and 22 vertical levels. It is driven by physical ocean fields (velocities, mixing, and temperature) from the IGSM climate model.[10] The model system was spun up for 2000 years using 1860 conditions. The Darwin model simulates inorganic and organic forms of carbon, nitrogen, phosphorus, iron, and silica, as well as six categories of phytoplankton functional groups (diatoms, other large, diazotrophs, coccolithophores, *Prochlorococcus* and *Synechococcus*; 16 species for each group and 96 in total). Two herbivorous zooplankton grazers with different sizes (small and large) are included in the ecology model. The two grazers feed preferentially on phytoplankton in two size classes (i.e., large zooplankton prefer the former four types; small zooplankton prefer the latter two). For this study, we use the monthly mean concentrations of dissolved organic carbon, particulate organic carbon, chlorophyll, and the biomass of different plankton types. We also use the monthly mean fluxes (or rates) of primary production, carbon remineralization, zooplankton grazing for each phytoplankton type, and mortality of zooplankton. For simplicity, we use the sum of the biomass of the 16 species of phytoplankton for each of the six function group.

The chemistry, transport, uptake, and trophic transfer of Hg chemicals is modeled using the MIT General Circulation Model for Hg (MITgcm-Hg), which is described and evaluated against available observations in Zhang et al.[6,46] Briefly, the model has a horizontal resolution of 1 ° × 1 ° with 50 vertical levels. The resolution is higher over equatorial regions (0.5 ° × 1 °) and the Arctic (~40 km). The atmospheric deposition, air-sea exchange, and riverine discharge

of Hg are considered following Zhang et al.[6,46]The ocean biogeochemistry and ecological variables are regridded from the Darwin model as described above. The model is driven by ocean state estimates between 1992 and 2011 by ECCO v4.[47] The impacts of future change in ocean physics on Hg cycling are not evaluated in this study because the Hg model is driven by present-day ocean physics. Although it is a discrepancy that the Darwin model was driven by ocean physics that includes the effect of climate change, the impact is of second order as we focus on the annual mean of the large-scale model state.

The Hg model includes the transformation of inorganic and organic Hg species with rate constants from previous model studies.[6] Four inorganic and organic Hg species, elemental Hg, inorganic divalent Hg, CH_3Hg, and $(CH_3)_2Hg$ are included in this model. The initial concentrations of ocean Hg species are taken from the previous model study, which was spun up for 10,000 years before simulating 1450 to 2008.[48] The methylation rate is scaled proportional to the organic carbon remineralization rate,[15,49] while the demethylation rate is a function of sunlight and temperature. CH_3Hg is taken up by phytoplankton based on their volume concentration factor (defined as the ratio of CH_3Hg concentrations in phytoplankton and seawater) as a function of cell diameter and local seawater dissolved organic carbon concentration following the parameterization developed by Schartup et al.[8] Uptake is represented as a fast equilibrium process because a steady state was reached within hours in controlled experiments.[7,43] The trophic transfer of CH_3Hg from phytoplankton to zooplankton is calculated based on the grazing flux, phytoplankton biomass, and CH_3Hg concentrations. The return of unassimilated CH_3Hg in zooplankton to seawater via zooplankton elimination and mortality are also included.

We perform a simulation that uses the output of the Darwin model driven by IGSM for the year 2000 to represent a baseline condition.[10] The second simulation allows physical factors such as temperature, circulation, and sea-ice to change from 2000 to 2100 in the IGSM. In a third simulation, we consider the response of phytoplankton to ocean acidification on top of the physical factors in the second simulation. The model is run for 10 years for each scenario and the result for the last year is used for data analysis, as this time is sufficient for the distribution of Hg species at the top 500 m to adjust to changes in ocean biogeochemistry (Figure S5).[6]

SUPPLEMENTAL INFORMATION

Supplemental Information can be found online at https://doi.org/10.1016/j.oneear.2021.01.005.

ACKNOWLEDGMENTS

Y.Z. acknowledges financial support from the National Natural Science Foundation of China (NNSFC) 41875148, start-up funds from the Thousand Youth Talents Plan, Jiangsu Innovative and Entrepreneurial Talents Plan, and the Collaborative Innovation Center of Climate Change, Jiangsu Province. E.M.S. acknowledges funding from the U.S. National Science Foundation (OCE 1260464). S.D. acknowledges funding support from NASA (80NSSC17K0561). We acknowledge Katlin Bowman, Feiyue Wang, Carl Lamborg, Michelle Nerentorp, and Katarina Gårdfeldt for providing observational datasets. We thank all the scientists who have participated in the collection and analysis of the observation data used in this study. The authors also thank Lars-Eric Heimbürger-Boavida and two anonymous reviewers for their helpful comments and suggestions.

AUTHOR CONTRIBUTIONS

Y.Z. and E.M.S. designed the study; Y.Z. performed the study; S.D. provided the ocean biogeochemical dataset; and Y.Z., S.D., and E.M.S. wrote the paper.

DECLARATION OF INTERESTS

The authors declare no competing interests.

Received: March 26, 2020
Revised: October 27, 2020
Accepted: January 19, 2021
Published: February 5, 2021

REFERENCES

1. Debes, F., Weihe, P., and Grandjean, P. (2016). Cognitive deficits at age 22 years associated with prenatal exposure to methylmercury. Cortex *74*, 358–369.
2. Roman, H.A., Walsh, T.L., Coull, B.A., Dewailly, É., Guallar, E., Hattis, D., Mariën, K., Schwartz, J., Stern, A.H., Virtanen, J.K., et al. (2011). Evaluation of the cardiovascular effects of methylmercury exposures: current evidence supports development of a dose-response function for regulatory benefits analysis. Environ. Health Perspect. *119*, 607–614.
3. Eagles-Smith, C.A., Silbergeld, E.K., Basu, N., Bustamante, P., Diaz-Barriga, F., Hopkins, W.A., Kidd, K.A., and Nyland, J.F. (2018). Modulators of mercury risk to wildlife and humans in the context of rapid global change. Ambio *47*, 170–197.
4. Sunderland, E.M., Li, M., and Bullard, K. (2018). Erratum: "decadal changes in the edible supply of seafood and methylmercury exposure in the United States. Environ. Health Perspect. *126*, 029003.
5. Obrist, D., Kirk, J.L., Zhang, L., Sunderland, E.M., Jiskra, M., and Selin, N.E. (2018). A review of global environmental mercury processes in response to human and natural perturbations: changes of emissions, climate, and land use. Ambio *47*, 116–140.
6. Zhang, Y., Soerensen, A.L., Schartup, A.T., and Sunderland, E.M. (2020). A global model for methylmercury formation and uptake at the base of marine food webs. Glob. Biogeochem. Cycles *34*, 1–21.
7. Lee, C.S., and Fisher, N.S. (2016). Methylmercury uptake by diverse marine phytoplankton. Limnol. Oceanogr. *61*, 1626–1639.
8. Schartup, A.T., Qureshi, A., Dassuncao, C., Thackray, C.P., Harding, G., and Sunderland, E.M. (2018). A model for methylmercury uptake and trophic transfer by marine plankton. Environ. Sci. Technol. *52*, 654–662.
9. Marinov, I., Doney, S.C., and Lima, I.D. (2010). Response of ocean phytoplankton community structure to climate change over the 21st century: partitioning the effects of nutrients, temperature and light. Biogeosciences *7*, 3941–3959.
10. Dutkiewicz, S., Morris, J.J., Follows, M.J., Scott, J., Levitan, O., Dyhrman, S.T., and Berman-Frank, I. (2015). Impact of ocean acidification on the structure of future phytoplankton communities. Nat. Clim. Chang. *5*, 1002–1006.
11. Dutkiewicz, S., Scott, J.R., and Follows, M.J. (2013). Winners and losers: ecological and biogeochemical changes in a warming ocean. Glob. Biogeochem. Cycles *27*, 463–477.
12. Krabbenhoft, D.P., and Sunderland, E.M. (2013). Global change and mercury. Science *341*, 1457–1458.
13. Booth, S., and Zeller, D. (2005). Mercury, food webs, and marine mammals: implications of diet and climate change for human health. Environ. Health Perspect. *113*, 521–526.
14. Downs, S.G., Macleod, C.L., and Lester, J.N. (1998). Mercury in precipitation and its relation to bioaccumulation in fish: a literature review. Water Air Soil Pollut. *108*, 149–187.
15. Sunderland, E.M., Krabbenhoft, D.P., Moreau, J.W., Strode, S.A., and Landing, W.M. (2009). Mercury sources, distribution, and bioavailability in the North Pacific Ocean: insights from data and models. Glob. Biogeochem. Cycles *23*, 1–14.
16. Cossa, D., Averty, B., and Pirrone, N. (2009). The origin of methylmercury in open mediterranean waters. Limnol. Oceanogr. *54*, 837–844.
17. Cossa, D., Heimbürger, L.E., Lannuzel, D., Rintoul, S.R., Butler, E.C.V., Bowie, A.R., Averty, B., Watson, R.J., and Remenyi, T. (2011). Mercury in the Southern Ocean. Geochim. Cosmochim. Acta *75*, 4037–4052.
18. Gilmour, C.C., Podar, M., Bullock, A.L., Graham, A.M., Brown, S.D., Somenahally, A.C., Johs, A., Hurt, R.A., Bailey, K.L., and Elias, D.A. (2013). Mercury methylation by novel microorganisms from new environments. Environ. Sci. Technol. *47*, 11810–11820.
19. Gionfriddo, C.M., Tate, M.T., Wick, R.R., Schultz, M.B., Zemla, A., Thelen, M.P., Schofield, R., Krabbenhoft, D.P., Holt, K.E., and Moreau, J.W.

(2016). Microbial mercury methylation in Antarctic sea ice. Nat. Microbiol. *1*, 1–12.

20. Villar, E., Cabrol, L., and Heimbürger-Boavida, L.E. (2020). Widespread microbial mercury methylation genes in the global ocean. Environ. Microbiol. Rep. *12*, 277–287.
21. Stern, G.A., Macdonald, R.W., Outridge, P.M., Wilson, S., Chételat, J., Cole, A., Hintelmann, H., Loseto, L.L., Steffen, A., Wang, F., et al. (2012). How does climate change influence arctic mercury? Sci. Total Environ. *414*, 22–42.
22. Jonsson, S., Andersson, A., Nilsson, M.B., Skyllberg, U., Lundberg, E., Schaefer, J.K., Åkerblom, S., and Björn, E. (2017). Terrestrial discharges mediate trophic shifts and enhance methylmercury accumulation in estuarine biota. Sci. Adv. *3*, 1–10.
23. Hansell, D.A., Carlson, C.A., Repeta, D.J., and Schlitzer, R. (2009). Dissolved organic matter in the ocean a controversy stim ulates new insights. Oceanography *22*, 202–211.
24. Zeller, D., and Reinert, J. (2004). Modelling spatial closures and fishing effort restrictions in the Faroe Islands marine ecosystem. Ecol. Modell. *172*, 403–420.
25. Alava, J.J., Cisneros-Montemayor, A.M., Sumaila, U.R., and Cheung, W.W.L. (2018). Projected amplification of food web bioaccumulation of MeHg and PCBs under climate change in the Northeastern Pacific. Sci. Rep. *8*, 1–12.
26. Schartup, A.T., Thackray, C.P., Qureshi, A., Dassuncao, C., Gillespie, K., Hanke, A., and Sunderland, E.M. (2019). Climate change and overfishing increase neurotoxicant in marine predators. Nature *572*, 648–650.
27. Moss, R.H., Edmonds, J.A., Hibbard, K.A., Manning, M.R., Rose, S.K., Van Vuuren, D.P., Carter, T.R., Emori, S., Kainuma, M., Kram, T., et al. (2010). The next generation of scenarios for climate change research and assessment. Nature *463*, 747–756.
28. Bowman, K.L., Lamborg, C.H., and Agather, A.M. (2020). A global perspective on mercury cycling in the ocean. Sci. Total Environ. *710*, 136166.
29. Bopp, L., Aumont, O., Cadule, P., Alvain, S., and Gehlen, M. (2005). Response of diatoms distribution to global warming and potential implications: a global model study. Geophys. Res. Lett. *32*, 1–4.
30. Steinacher, M., Joos, F., Frölicher, T.L., Bopp, L., Cadule, P., Doney, S.C., Gehlen, M., Schneider, B., and Segschneider, J. (2009). Projected 21st century decrease in marine productivity: a multi-model analysis. Biogeosci. Discuss *6*, 7933–7981.
31. Fisher, J.A., Jacob, D.J., Soerensen, A.L., Amos, H.M., Corbitt, E.S., Streets, D.G., Wang, Q., Yantosca, R.M., and Sunderland, E.M. (2013). Factors driving mercury variability in the Arctic atmosphere and ocean over the past 30 years. Glob. Biogeochem. Cycles *27*, 1226–1235.
32. Fisher, J.A., Jacob, D.J., Soerensen, A.L., Amos, H.M., Steffen, A., and Sunderland, E.M. (2012). Riverine source of Arctic Ocean mercury inferred from atmospheric observations. Nat. Geosci. *5*, 499–504.
33. DiMento, B.P., Mason, R.P., Brooks, S., and Moore, C. (2019). The impact of sea ice on the air-sea exchange of mercury in the Arctic Ocean. Deep. Res. Part Oceanogr. Res. Pap. *144*, 28–38.
34. Sonke, J.E., Teisserenc, R., Heimbürger-Boavida, L.E., Petrova, M.V., Marusczak, N., Le Dantec, T., Chupakov, A.V., Li, C., Thackray, C.P., Sunderland, E.M., et al. (2018). Eurasian river spring flood observations support net Arctic Ocean mercury export to the atmosphere and Atlantic Ocean. Proc. Natl. Acad. Sci. U S A *115*, E11586–E11594.
35. Schaefer, K., Elshorbany, Y., Jafarov, E., Schuster, P.F., Striegl, R.G., Wickland, K.P., and Sunderland, E.M. (2020). Potential impacts of mercury released from thawing permafrost. Nat. Commun. *11*, 1–6.
36. Schuster, P.F., Schaefer, K.M., Aiken, G.R., Antweiler, R.C., Dewild, J.F., Gryziec, J.D., Gusmeroli, A., Hugelius, G., Jafarov, E., Krabbenhoft, D.P., et al. (2018). Permafrost stores a globally significant amount of mercury. Geophys. Res. Lett. *45*, 1463–1471.
37. Lim, A.G., Jiskra, M., Sonke, J.E., Loiko, S.V., Kosykh, N., and Pokrovsky, O.S. (2020). A revised pan-Arctic permafrost soil Hg pool based on Western Siberian peat Hg and carbon observations. Biogeosciences *17*, 3083–3097.
38. Kwon, E.Y., Primeau, F., and Sarmiento, J.L. (2009). The impact of remineralization depth on the air-sea carbon balance. Nat. Geosci. *2*, 630–635.
39. Eberlein, T., Van de Waal, D.B., and Rost, B. (2014). Differential effects of ocean acidification on carbon acquisition in two bloom-forming dinoflagellate species. Physiol. Plant *151*, 468–479.
40. Lohbeck, K.T., Riebesell, U., and Reusch, T.B.H. (2012). Adaptive evolution of a key phytoplankton species to ocean acidification. Nat. Geosci. *5*, 346–351.
41. Dutkiewicz, S., Follows, M.J., and Bragg, J.G. (2009). Modeling the coupling of ocean ecology and biogeochemistry. Glob. Biogeochem. Cycles *23*, 1–15.
42. Kirk, J.L., Lehnherr, I., Andersson, M., Braune, B.M., Chan, L., Dastoor, A.P., Durnford, D., Gleason, A.L., Loseto, L.L., Steffen, A., et al. (2012). Mercury in Arctic marine ecosystems: sources, pathways and exposure. Environ. Res. *119*, 64–87.
43. Kim, H., Duong, H.V., Kim, E., Lee, B.G., and Han, S. (2014). Effects of phytoplankton cell size and chloride concentration on the bioaccumulation of methylmercury in marine phytoplankton. Environ. Toxicol. *29*, 936–941.
44. Hammerschmidt, C.R., Finiguerra, M.B., Weller, R.L., and Fitzgerald, W.F. (2013). Methylmercury accumulation in plankton on the continental margin of the northwest atlantic ocean. Environ. Sci. Technol. *47*, 3671–3677.
45. Chust, G., Allen, J.I., Bopp, L., Schrum, C., Holt, J., Tsiaras, K., Zavatarelli, M., Chifflet, M., Cannaby, H., Dadou, I., et al. (2014). Biomass changes and trophic amplification of plankton in a warmer ocean. Glob. Chang. Biol. *20*, 2124–2139.
46. Zhang, Y., Jacob, D.J., Dutkiewicz, S., Amos, H.M., Long, M.S., and Sunderland, E.M. (2015). Biogeochemical drivers of the fate of riverine mercury discharged to the global and Arctic oceans. Global Biogeochemical Cycles *29*, 854–864.
47. Forget, G., Campin, J.M., Heimbach, P., Hill, C.N., Ponte, R.M., and Wunsch, C. (2015). ECCO version 4: an integrated framework for nonlinear inverse modeling and global ocean state estimation. Geosci. Model. Dev. *8*, 3071–3104.
48. Zhang, Y., Jaeglé, L., and L T. (2014). Natural biogeochemical cycle of mercury in a global three-dimensional ocean tracer model. Glob. Biogeochem. Cycles *28*, 553–570.
49. Ortiz, V.L., Mason, R.P., and Evan Ward, J. (2015). An examination of the factors influencing mercury and methylmercury particulate distributions, methylation and demethylation rates in laboratory-generated marine snow. Mar. Chem. *177*, 753–762.